THE JOURNAL OF BIOLOGICAL CHEMISTRY VOL. 286, NO. 3, pp. 1876–1883, January 21, 2011

Paired Immunoglobulin-like Receptor B Knockout Does Not Enhance Axonal Regeneration or Locomotor Recovery after Spinal Cord Injury*[S]

Received for publication, July 12, 2010, and in revised form, November 16, 2010 Published, JBC Papers in Press, November 18, 2010, DOI 10.1074/jbc.M110.163493

Yuka Nakamura[‡§], **Yuki Fujita**[‡§], **Masaki Ueno**[‡§], **Toshiyuki Takai**[¶], **and Toshihide Yamashita**[‡§1]

From the [‡]*Department of Molecular Neuroscience, Graduate School of Medicine, Osaka University, 2-2 Yamadaoka, Suita, Osaka 565-0871, Japan,* [§]*Japan Science and Technology Agency, CREST, 5, Sanbancho, Chiyoda-ku, Tokyo 102-0075, Japan, and* [¶]*Department of Experimental Immunology and JST, CREST, Institute of Development, Aging, and Cancer, Tohoku University, 4-1 Seiryo, Sendai, Miyagi 980-8575, Japan*

Myelin components that inhibit axonal regeneration are believed to contribute significantly to the lack of axonal regeneration noted in the adult central nervous system. Three proteins found in myelin, Nogo, myelin-associated glycoprotein, and oligodendrocyte-myelin glycoprotein, inhibit neurite outgrowth *in vitro*. All of these proteins interact with the same receptors, namely, the Nogo receptor (NgR) and paired immunoglobulin-like receptor B (PIR-B). As per previous reports, corticospinal tract (CST) regeneration is not enhanced in NgR-knock-out mice after spinal cord injury. Therefore, we assessed CST regeneration in PIR-B-knock-out mice. We found that hindlimb motor function, as assessed using the Basso mouse scale, footprint test, inclined plane test, and beam walking test, did not differ between the PIR-B-knock-out and wild-type mice after dorsal hemisection of the spinal cord. Further, tracing of the CST fibers after injury did not reveal enhanced axonal regeneration or sprouting in the CST of the PIR-B-knock-out mice. Systemic administration of NEP1–40, a NgR antagonist, to PIR-B knock-out mice did not enhance the regenerative response. These results indicate that PIR-B knockout is not sufficient to induce extensive axonal regeneration after spinal cord injury.

Various factors can hamper axonal regeneration after spinal cord injury (SCI),[2] including the reduced propensity for growth shown by the axons of the adult CNS (1). Three myelin-associated proteins, namely, myelin-associated glycoprotein (MAG), Nogo, and oligodendrocyte-myelin glycoprotein (OMgp), potently inhibit neurite growth *in vitro*. Although these myelin inhibitors exhibit marked structural variations, they all interact with the Nogo receptor (NgR). Therefore, NgR has been considered a good molecular target for the treatment of CNS injuries. Indeed, RhoA, one of the key signals downstream of NgR, has been shown to be activated spatially around the injured site after SCI (2). Two research groups have conducted studies on NgR knock-out: one group reported that this mutation abolished the growth cone collapse response to myelin inhibitors, allowed for a limited amount of regeneration of the raphespinal and rubrospinal tracts, but did not enable the regeneration of the corticospinal tract (CST) after SCI (3). However, the other research group found that myelin inhibitors inhibited neurite growth to the same extent in the neurons of both NgR-knock-out mice and wild-type mice and completely inhibited CST regeneration after SCI in NgR-knock-out mice (4). In the latter study, neurons were cultured, and it was found that Nogo-66, which comprises one of the two inhibitory domains of Nogo carried by a chain of 66 amino acids, inhibited neurite growth to the same extent in the NgR-knock-out mice as in the wild-type mice. This finding strongly suggested the existence of additional receptors, apart from NgR, that interact with myelin inhibitors.

Subsequently, another such receptor, paired immunoglobulin-like receptor B (PIR-B), was identified (5). This receptor was first described in terms of its activity in the immune system. PIR-B is an MHC class I receptor (6) and contains immunoreceptor tyrosine-based inhibitory motifs. Phosphorylation of these sites stimulates the binding of Shp-1 and Shp-2 phosphatases to PIR-B, and this binding in turn modulates the signal transduction pathways operating in the immune system. PIR-B is expressed on cells of various hematopoietic lineages as well as on neurons (7). It binds not only to Nogo-66 but also to MAG and OMgp and is partly responsible for the effects of Nogo-66 and total myelin in inhibiting neurite growth (5). Interestingly, PIR-B inhibition by a neutralizing antibody in NgR-null cerebellar neurons completely abrogated the effects of total myelin in inhibiting neurite growth. This finding suggests that NgR and PIR-B may be responsible for transducing all of the inhibitory signals produced by total myelin. However, it remains unclear as to whether PIR-B inhibition is sufficient for inducing axonal regeneration *in vivo*. In the present study, we assessed the role of PIR-B in the failure of regeneration *in vivo* by using PIR-B-knock-out mice.

* This work was supported by a grant-in-aid for young scientists from the Japan Society for the Promotion of Science.

[S] The on-line version of this article (available at http://www.jbc.org) contains supplemental Materials and Methods, additional references, and Fig. 1.

[1] To whom correspondence should be addressed: Dept. of Molecular Neuroscience, Graduate School of Medicine, Osaka University, 2-2 Yamadaoka, Suita, Osaka 565-0871, Japan. Tel.: 81-6-68793661; Fax: 81-6-68793669; E-mail: yamashita@molneu.med.osaka-u.ac.jp.

[2] The abbreviations used are: SCI, spinal cord injury; BDA, biotinylated dextran amine; BMS, Basso mouse scale; CST, corticospinal tract; MAG, myelin-associated glycoprotein; NgR, Nogo receptor; Omgp, oligodendrocyte-myelin glycoprotein; PIR-B, paired immunoglobulin-like receptor B.

EXPERIMENTAL PROCEDURES

Mice—C57BL/6J mice (age, 8 weeks) were purchased from Charles River Laboratories and were bred and maintained at the Institute of Experimental Animal Sciences, Osaka University Graduate School of Medicine. PIR-B$^{-/-}$ mice were generated as described previously (8) and backcrossed with C57BL/6J mice. All experimental procedures were approved by the Institutional Ethics Committee of Osaka University.

Surgical Procedures for Inducing SCI—Mice (body weight, 16.5–25.5 g) were anesthetized with sodium pentobarbital (50 mg/kg). The skin over the thoracic vertebrae was shaved and cleaned with an iodine tincture. The skin was incised, and the connective and muscle tissues were bluntly dissected to expose the lower thoracic spinal cord. T9 laminectomy was performed, ensuring that the spinal cord was not damaged during the removal of the dorsal lamina. The dura was cut with a needle. Further, the surgical microknife was used to perform dorsal hemisection at T9, ensuring that the dorsal and dorsolateral CSTs were severed to a depth of 1.0 mm. To ensure that the lesion was laterally complete, the surgical microknife was passed through the dorsal part of the spinal cord several times with a view to creating a lesion that extended downward to the central canal.

NEP1–40 Treatment—NEP1–40 treatment was performed as described previously (9). The animals were administered NEP1–40 (Merck), an NgR antagonist peptide (10), with an intrapenitoreal injection ($n = 17$ for wild-type, and $n = 6$ for PIR-B$^{-/-}$ mice) or an intrathecal administration ($n = 7$) with an implanted osmotic minipump (model 2002; Alzet, Cupertino, CA). For intraperitoneal injections, 100 μl of NEP1–40 dissolved in the vehicle (83% PBS + 17% dimethyl sulfoxide) at a final concentration of 2.088 mg/ml was administered at 3 h after induction of SCI and then once daily for 14 days. This represents an approximate dose of 11.6 mg/kg per day. For the intrathecal administration, a pump connected to a silicone tube was filled with vehicle (83% PBS, 17% dimethyl sulfoxide) or NEP1–40 in the vehicle. After SCI, the pump was implanted in the subcutaneous space, and the tube was indwelled into the injury site for the local administration. The vehicle and NEP1–40 were delivered continuously at rate of 0.6 μl/h for 14 days (11.6 mg/kg per day).

Behavioral Assessment—All animals were subjected to four motor tests, the Basso mouse scale (BMS), inclined plane, beam walking, and footprint test, to evaluate the functional recovery of hindlimbs after SCI (see supplemental Materials and Methods). Those tests were conducted the day before the surgery to evaluate the normal performance of mice. For beam walking tests, the mice were trained to walk on a narrow beam prior to injury.

Immunoprecipitation Assay—Mouse cortex, spinal cord, and spleen were lysed in 50 mM Tris-HCl (pH 7.5), 150 mM NaCl, 1% Nonidet P-40, 1 mM EDTA, and 2 mM sodium orthovanadate supplemented with proteinase inhibitors (Roche Applied Science). The lysates were centrifuged at 17,000 × *g* at 4 °C for 10 min, and the protein concentrations of the supernatants were measured and normalized among the samples. As an internal control, a fraction of lysates with equal amounts of proteins were boiled in sample buffer containing 5% β-mercaptoethanol for 5 min and subjected to SDS-PAGE. The rest of lysates with equal amounts of proteins were sequentially incubated with rat anti-mouse PIR (BD Pharmingen) and protein G-conjugated Sepharose (GE Healthcare). The resultant beads were washed four times, and boiled in sample buffer. The protein samples were subjected to SDS-PAGE and transblotted to PVDF membranes. The membranes were incubated with goat anti-mouse PIR-B (1:400; Santa Cruz Biotechnology, Santa Cruz, CA) or mouse anti-α-tubulin antibody (for the control, 1:1000; Santa Cruz Biotechnology). HRP-conjugated secondary antibodies and ECL Plus reagents (GE Healthcare) were used for detection. Membranes were exposed to an image system (LAS-3000; Fujifilm, Tokyo, Japan) according to the manufacturer's specifications.

Histological Analysis—The mice were perfused transcardially with PBS followed by 4% paraformaldehyde in 0.1 M phosphate buffer. The spinal cords were dissected, postfixed in the same fixatives, and immersed overnight in PBS containing 30% sucrose. The spinal cords were then embedded in Tissue-Tek OCT and kept frozen at −80 °C until use. Serial parasagittal sections and transverse sections (20 μm thick) were cut on a cryostat and mounted on Matsunami adhesive silane-coated Superfrost/Plus slides (Matsunami, Osaka, Japan). The sections were washed three times with PBS and blocked in PBS supplemented with 5% BSA and 0.1% Triton X-100 for 1 h at room temperature. We performed immunostaining for glial fibrillary acidic protein to visualize glial scar formation as an indicator of the lesion depth at the epicenter. The sections were incubated overnight at 4 °C with a polyclonal anti-PIR-B antibody (1:250; Lilrb3, A-20; Santa Cruz Biotechnology) or a monoclonal anti-glial fibrillary acidic protein antibody (1: 200; Sigma). They were then washed three times with PBS and incubated with Alexa Fluor 488-conjugated secondary antibodies (1:500; Invitrogen) for 1 h at room temperature. In some cases, Alexa Fluor 568-conjugated streptavidin (1:400; Invitrogen) was used for coimmunostaining. The samples were examined under a fluorescence microscope (Olympus BX51, DP71).

Quantification—To quantify regeneration and sprouting of the CST, biotinylated dextran amine (BDA), an anterograde tracer, was injected into the right sensorimotor cortex 4 weeks after the induction of SCI, and the CST was visualized on frozen sections (see supplemental Materials and Methods). The distance from the end of the main bundles in the CST to the lesion epicenter was measured for each animal to quantify the retraction of the CST fibers. For this measurement, we used the sagittal sections (extending 5 mm rostral and 5 mm caudal to the lesion epicenter) cut in the plane through which the axon bundles in the main dorsal CST ran. The distance between the lesion epicenter and the tips of the injured CST axons (bulbous in appearance) was measured and averaged (10 axons per section). The distance rostral to the lesion epicenter was considered positive distance.

To quantify axonal sprouting and regeneration in the CST, we obtained serial transverse sections of the spinal cord and quantitatively analyzed the axonal distribution. The degree of BDA uptake was assessed by counting the pixels in the BDA-labeled fibers in the normal dorsal CST area; for this assess-

ment, we used the Scion Image software (Scion Corporation) and transverse sections from 5 mm rostral to the lesion site. To quantify the labeled CST axons in the region from 5 mm rostral to 5 mm caudal to the lesion site, the pixels in the labeled fibers of the gray matter or the dorsal CST were counted for each animal, and this value was divided by the number of pixels in the labeled dorsal CST axons located 5 mm above the lesion. The lesion depth from the dorsal surface of the spinal cord was measured in sagittal sections containing the lesion epicenter after immunostaining with the anti-glial fibrillary acidic protein antibody.

Statistical Analysis—Statistical analyses were described in the figure legends. *p* values of less than 0.05 were considered significant.

RESULTS

PIR-B Expression Is increased after SCI—PIR-B is reported to be expressed in the adult brain, including the cerebral cortex (7); thus, the spatial expression of PIR-B should reflect its role in mediating the responses of corticospinal neurons to inhibitory cues after SCI. At first, we examined expression of PIR-B in the cerebral cortex and the spinal cord. An immunoprecipitation assay revealed that PIR-B was expressed in the cerebral cortex and the spinal cord as well as the spleen (Fig. 1*A*). To confirm that the signal in the Western blot was specific to PIR-B, we employed PIR-B$^{-/-}$ mice. PIR-B$^{-/-}$ mice were generated by standard gene-targeting methods that resulted in the deletion of sequences encoding the sixth ectodomain and juxtamembrane domain of the protein (8). As expected, no bands for PIR-B were visible in any tissues from PIR-B$^{-/-}$ mice (Fig. 1*A*). We next assessed whether PIR-B expression was altered in these tissues after SCI. Although the expression of PIR-B appeared to be increased in the cerebral cortex after thoracic SCI (Fig. 1*B*), it was not statistically significant. However, the PIR-B expression was significantly induced around the injured site in the spinal cord at 3 days after SCI (Fig. 1*C*). These results suggest some function of PIR-B in the pathogenesis of SCI.

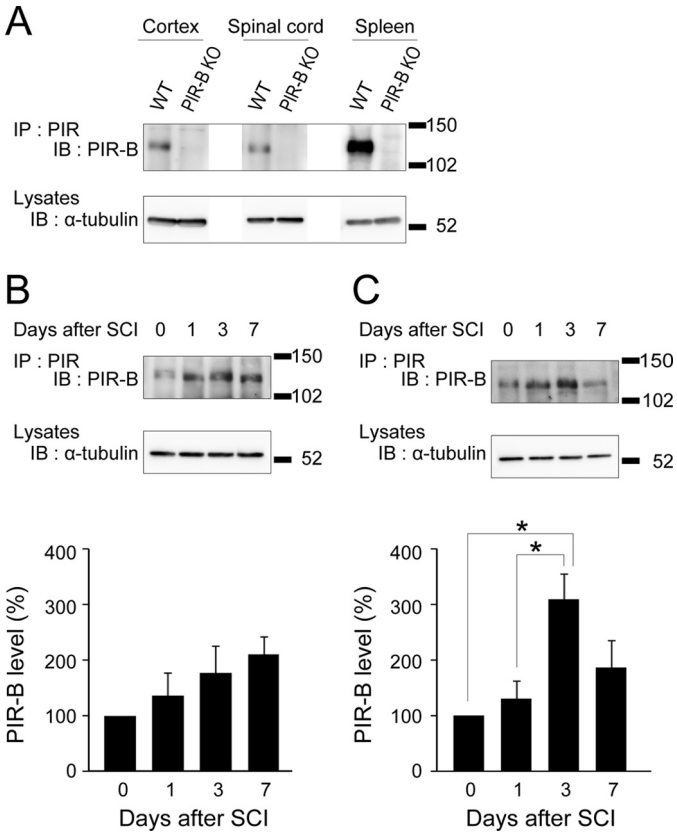

FIGURE 1. **PIR-B expression is increased after SCI.** *A*, immunoprecipitation (*IP*) assay revealed that PIR-B was expressed in cortex, spinal cord, and spleen. PIR-B protein was immunoprecipitated from each tissue of wild-type (*WT*) or PIR-B$^{-/-}$ (*PIR-B KO*) mice with equal amounts of protein. *IB*, immunoblotting. α-Tubulin is an internal control. *B*, expression of PIR-B in the cerebral cortex at the indicated days after SCI is shown. The *graph* shows the relative PIR-B expression level compared with the control (day 0). *C*, expression of PIR-B in the spinal cord was enhanced after SCI. The *graph* shows the relative PIR-B expression level compared with the control (day 0). *B* and *C*, the data represent the mean ± S.E. (*error bars*), $n = 4$ for each group. *, $p < 0.05$ (one-way factorial ANOVA followed by Scheffe's multiple comparison test).

Recovery of Locomotor Activity after Dorsal Hemisection of the Spinal Cord Is Not Enhanced in PIR-B$^{-/-}$ Mice—The above results suggest a possibility that PIR-B may play a role in suppressing functional recovery after SCI. We used PIR-B$^{-/-}$ mice to assess whether functional recovery after SCI is more rapid in the absence of PIR-B. The PIR-B$^{-/-}$ mice did not exhibit any obvious abnormalities in locomotor activity as assessed by the BMS scores (data not shown). We created 1.0-mm-deep lesions in the dorsal region of the spinal cord at the T9 vertebral level by using a surgical microknife, ensuring transection of both the main and dorsolateral CSTs. Some of wild-type and PIR-B$^{-/-}$ mice received NEP1–40 systemically. At 6 weeks after the induction of SCI, we assessed the lesions by examining sagittal sections containing the lesion epicenters. We found that the lesion depth did not differ significantly between the groups (see Fig. 3*M*). We evaluated the hindlimb locomotor function of the mice by recording BMS scores for up to 6 weeks after the induction of SCI. All of the injured mice became almost completely paraplegic on day 1 after the injury (Fig. 2*A*) but gradually began to display partial recovery of locomotor activity. In general, this recovery was slightly better in the PIR-B$^{-/-}$ mice than in the wild-type mice at a week after the injury, but this difference was not significant. Two-way repeated-measures ANOVA revealed that the overall BMS scores did not significantly differ between the PIR-B$^{-/-}$ and wild-type mice; furthermore, there were no significant differences between the two groups at any specific time point after the induction of SCI (Mann-Whitney *U* test; Fig. 2*A*). Thus, the recovery of locomotor activity after SCI was not significantly enhanced in the PIR-B$^{-/-}$ mice. In addition, the BMS scores recorded at any time points did not significantly differ among the NEP1–40-treated PIR-B$^{-/-}$, NEP1–40-treated wild-type mice, PIR-B$^{-/-}$, or the wild-type mice (Fig. 2*A*). As systemic administration of NEP1–40 was ineffective, we next delivered NEP1–40 intrathecally via osmotic minipumps for 2 weeks (11.6 mg/kg day day), and the locomotor performance of the animals was monitored for 6 weeks after the injury. The BMS scores recorded at any time points did not significantly differ between the NEP1–40-treated wild-type mice and the vehicle-treated wild-type mice (Fig. 2*B*). NEP1–40 efficiently silenced the growth cone-col-

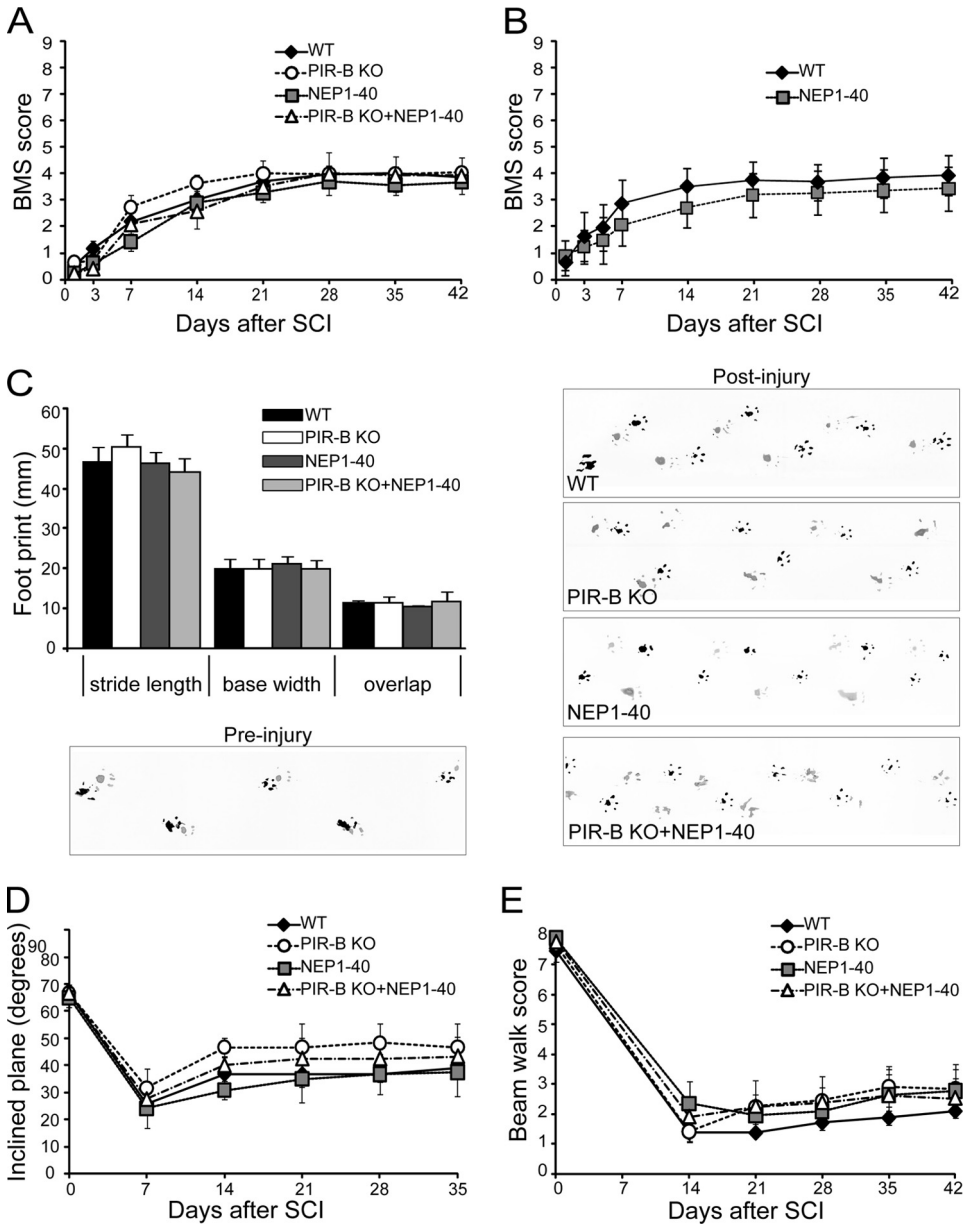

FIGURE 2. **The recovery of locomotor activity is not enhanced after SCI in PIR-B$^{-/-}$ mice.** *A*, the BMS scores (mean ± S.E. (*error bars*)) determined at the indicated time points after dorsal hemisection did not significantly differ among the wild-type (*WT*; $n = 16$), PIR-B$^{-/-}$ (*PIR-B KO*; $n = 15$), NEP1–40-treated wild-type (*NEP1–40*; $n = 17$), and NEP1–40-treated PIR-B$^{-/-}$ (*PIR-B KO + NEP1–40*; $n = 6$) mice. *B*, the BMS scores (mean ± S.E.) after dorsal hemisection did not significantly differ between the intrathecal NEP1–40-administered wild-type (*NEP1–40*; $n = 7$) and NEP1–40-untreated wild-type (*WT*; $n = 7$) mice. *C*, footprint analysis at 42 days after SCI reveals that stride length, base width, or overlap between forelimb and hindlimb placement did not significantly differ among the four groups. The *bottom* and *right panels* show examples of the representative footprints from preinjury control mice and each group of mice 42 days after SCI. Forelimb, *black*; hindlimb, *gray*. *D* and *E*, there was also no significant difference among the groups in the inclined plane test (*D*) or beam walking score (*E*). *C–E*, $n = 3–6$ for each group. *A*, *B*, *D*, and *E*, two-way repeated-measures ANOVA. *C*, one-way factorial ANOVA.

lapsing activity of Nogo-66 *in vitro* (supplemental Fig. 1*A*), confirming that NEP1–40 worked in our experiments. Hence, systemic administration of NEP1–40 produces outcome essentially identical to that with intrathecal administration as described previously (9, 10). Three other behavioral tests were used to characterize the performance of mice additionally. Analysis of hindpaw footprints in mice demonstrates that stride length, base width, or overlap between forelimb and hindlimb placement did not significantly differ among the four groups (Fig. 2*C*). There was also no significant difference among the groups in the inclined plane test (Fig. 2*D*), or beam walking test (Fig. 2*E*). These findings are in contrast to those reported by GrandPré *et al.* (10) but are consistent with the results of a subsequent study that reassessed the effects of NEP1–40 (11). We also confirmed that the neurite growth inhibition induced by Nogo-66 *in vitro* was suppressed in the cerebellar granule neurons from PIR-B$^{-/-}$ mice (supplemental Fig. 1*B*). Thus, neither the absence of PIR-B nor the inhibition of NgR enhanced the recovery of locomotor activity after dorsal hemisection of the mouse thoracic spinal cord in our experimental paradigm.

CST Regeneration after SCI Was Not Detectable in the PIR-B$^{-/-}$ Mice—Next, we examined axonal regeneration in the descending CST of the PIR-B$^{-/-}$ mice by injecting BDA

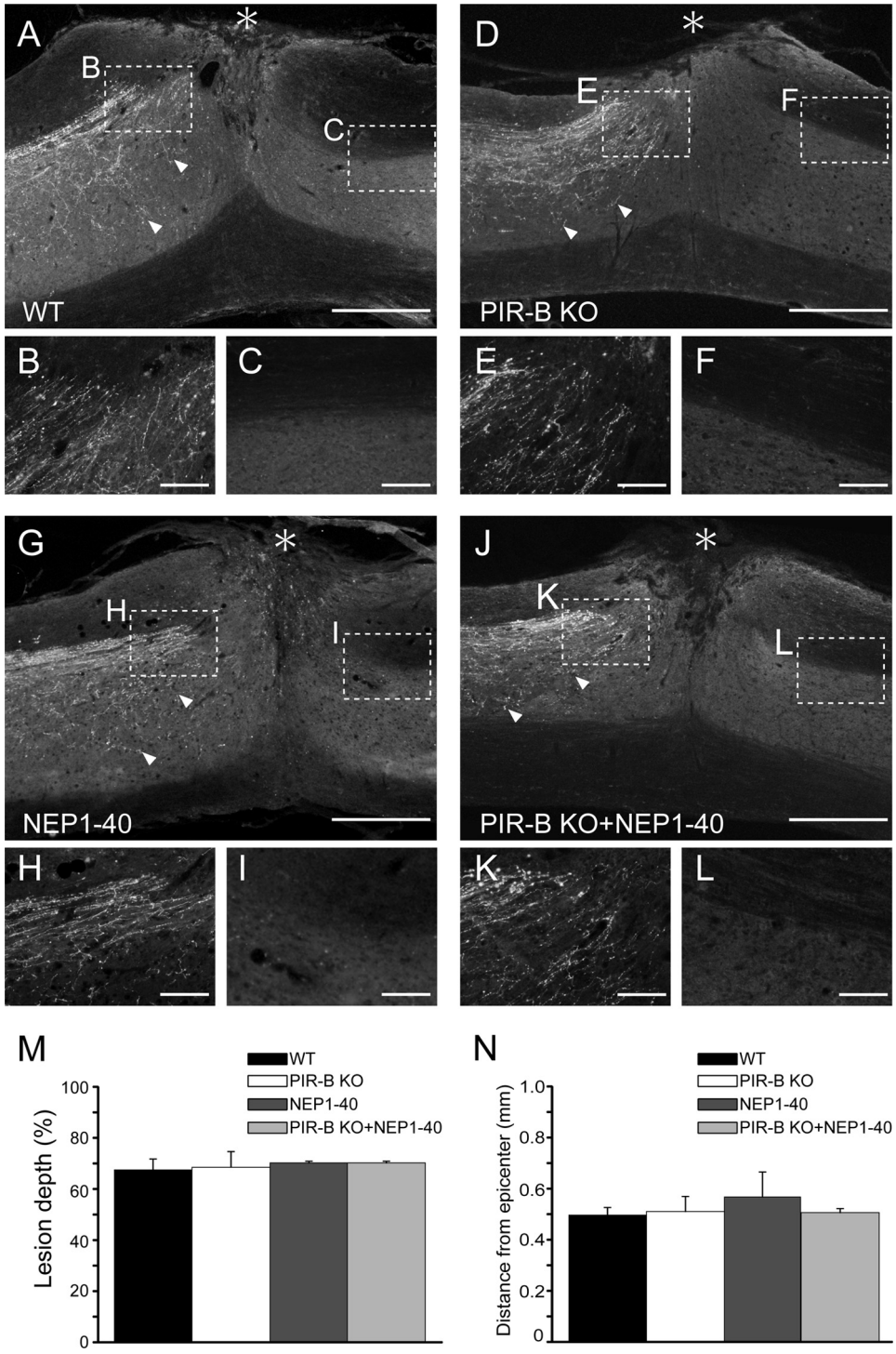

FIGURE 3. **Axonal regeneration/sprouting were not promoted in the CST after SCI in the PIR-B$^{-/-}$ mice.** *A*, *D*, *G*, and *J*, representative pictures of BDA-labeled CST fibers are shown. The rostral region is indicated to the *left*. Anterograde labeled CST fibers in the spinal cord of the WT (*A*), PIR-B KO (*D*), NEP1–40 (*G*), and PIR-B KO + NEP1–40 (*J*) mice at 6 weeks after SCI are shown. The lesion epicenter is indicated by an *asterisk*. In all groups of mice, numerous axon arbors were seen extending from the main CST into the gray matter rostral to the injury site (*arrowheads*). *B*, *C*, *E*, *F*, *H*, *I*, *K*, and *L*, higher magnifications of the *boxed regions* in *A*, *D*, *G*, and *J* are shown. *B*, *E*, *H*, and *K*, rostral regions contained many axons with retraction bulbs approaching the injury site. *C*, *F*, *I*, and *L*, no obvious regenerating/sprouting fibers were noted in the caudal region of the spinal cord. *Scale bars*: 500 μm in *A*, *D*, *G*, and *J*; 100 μm in *B*, *C*, *E*, *F*, *H*, *I*, *K*, and *L*. *M*, Lesion depth (expressed as mean ± S.E. (*error bars*)) showed no statistically significant difference among the groups ($n = 3$ for PIR-B KO + NEP1–40, and four for other groups) using one-way factorial ANOVA. *N*, distance from the end of the axon bundles in the main CST to the lesion epicenter, as measured in longitudinal sections ($n = 4$ for WT, $n = 3$ for others), did not significantly differ among the groups as measured by the Kruskal-Wallis test.

into right sensorimotor cortices. The CST axons of these mice showed no abnormality (data not shown), indicating that PIR-B is not involved in CST development. During our surgical procedure, we transected both the main and lateral CSTs. Thus, all CST components were labeled by BDA injected into the sensorimotor cortex, as there is no evidence of ventral

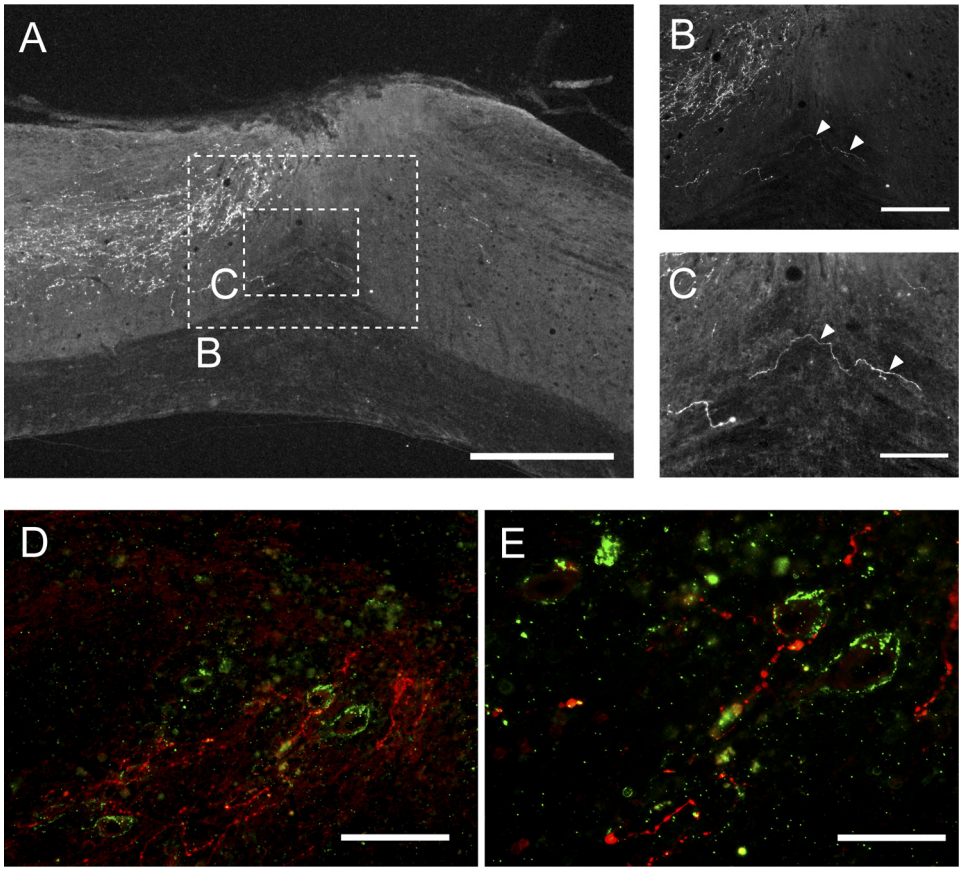

FIGURE 4. **The severed CST axons were in contact with interneurons expressing PIR-B in the spinal cord.** *A*, representative pictures of BDA-labeled CST fibers in the PIR-B$^{-/-}$ mice after SCI. The rostral region is indicated to the *left*. *B* and *C*, higher magnification of the *boxed regions* in *A*, showing extension of a few CST axons around and beyond the lesion. The *arrowheads* indicate axons extending from the gray matter into the ventral column. *D*, immunohistochemical analyses of BDA-positive fibers in the transected spinal cord. Representative photomicrographs are shown of sagittal sections obtained from the injury site of a wild-type mouse at 6 weeks after SCI. In the wild-type mice, the BDA-labeled fibers (*red*) were in contact with PIR-B-immunoreactive neurons (*green*) rostral to the lesion epicenter. *E*, higher magnification of *D*. *Scale bars*, 500 μm in *A*, 200 μm in *B*, 100 μm in *C* and *D*, 50 μm in *E*.

CST in C57BL/6J mice (11, 12). After the injection of BDA at 4 weeks after the surgery, the animals were kept alive for 2 more weeks. For some animals (three or four for each groups), sagittal plane sections of the main dorsal CST were cut from the region extending 5 mm rostral and 5 mm caudal to the lesion epicenter (Figs. 3 and 4). The far rostral and far caudal segments were sectioned in the transverse plane. For other animals (three for each groups), the spinal cord was sectioned in the transverse plane (Fig. 5). Sagittal sections through the lesion site revealed that the axon bundles in the main CST had retracted to the same extent in both the PIR-B$^{-/-}$ and wild-type mice (Fig. 3*N*). In both groups of mice, the main dorsal CST contained numerous retraction bulbs approaching the injury site, with a few axons extending closer (Fig. 3, *A*, *B*, *D*, and *E*). Further, we observed axon arbors extending from the main CST into the gray matter rostral to the lesion site in both the PIR-B$^{-/-}$ and wild-type mice (Fig. 3, *A* and *D*). However, the labeled fibers caudal to the lesion epicenter could not be detected in either the PIR-B$^{-/-}$ or wild-type mice (Fig. 3, *C* and *F*). Consistent with a previous report (12), in the case of both the PIR-B$^{-/-}$ mice (Fig. 4, *A*–*C*) and the wild-type mice (data not shown), only a few BDA-labeled CST axons could be seen extending from the gray matter rostral to the lesion site, in the direction of the ventral column and beyond the lesion. Interestingly, in the wild-type mice, the BDA-labeled fibers were in contact with PIR-B-immunoreactive neuronal cells around the lesions (Fig. 4, *D* and E). These results indicate that PIR-B may be expressed in the interneurons in the spinal cord as well as the pyramidal neurons in the cerebral cortex (7, 13).

The axon bundles in the main CST exhibited a similar degree of retraction in both the NEP1–40-treated wild-type and NEP1–40-treated PIR-B$^{-/-}$ mice compared with the wild-type mice (Fig. 3*N*). In addition, we could not detect signs indicative of a regenerative response in these mice (Fig. 3, *G*–*L*).

Because examination of the sagittal sections did not reveal any obvious regenerative responses in the PIR-B$^{-/-}$ mice beyond those in the wild-type mice, we decided to analyze the axonal distribution quantitatively by using transverse sections of the spinal cord. The total number of labeled fibers located 5 mm above the lesion was almost identical in all groups of mice (Fig. 5, *A*, *C*, *E*, *G*, and *I*); this indicated that the extent of BDA uptake was similar in all groups. We examined and compared the regenerative responses of the CST fibers in three mice per group, and representative sections of one animal per group are shown in Fig. 5. In all groups, extensive collaterals were detected in the gray matter rostral to the lesion epicen-

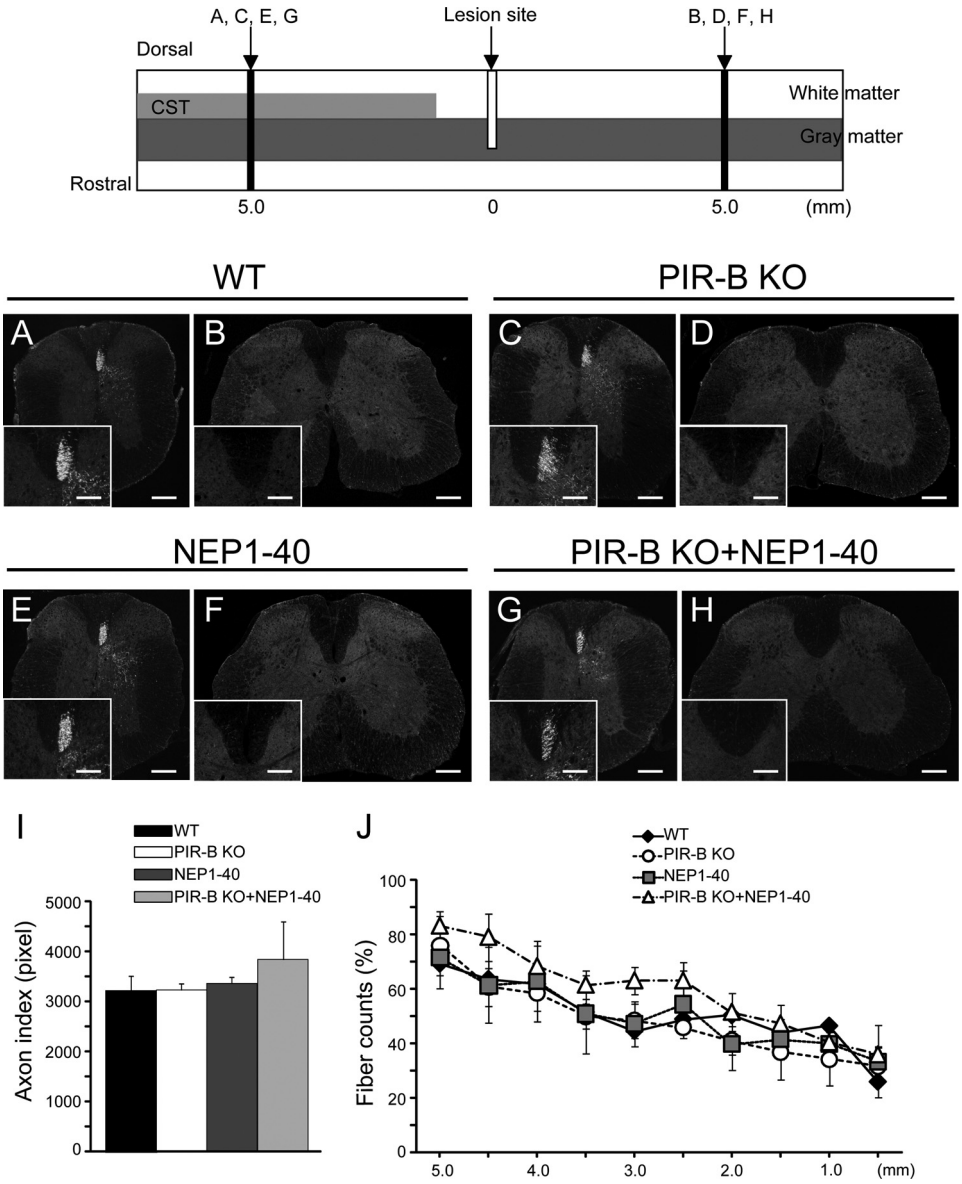

FIGURE 5. **Distribution of the sprouting CST fibers in the spinal cord.** *Top*, injured spinal cord illustrated schematically. *A–H*, representative transverse sections of the spinal cord obtained from 5 mm rostral (*A*, *C*, *E*, and *G*) or 5 mm caudal (*B*, *D*, *F*, and *H*) to the lesion site in the WT (*A* and *B*), PIR-B KO (*C* and *D*), NEP1–40 (*E* and *F*), and PIR-B KO + NEP1–40 (*G* and *H*) mice. *Insets*, high magnification views of dorsal funiculus. *Scale bars*, 200 μm in *A–H*; 100 μm in *insets*. *I*, pixel number of labeled corticospinal axons 5 mm rostral to the lesion site. The numbers did not significantly differ among the groups (using one-way factorial ANOVA). *J*, quantification of the extent of regeneration. The *x axis* represents specific locations along the rostrocaudal axis of the spinal cord; the *y axis* (axon index) indicates the ratio of the average pixel number of axons at each rostrocaudal location outside the main CST to the pixel number of the labeled fibers in the region 5 mm rostral to the lesion epicenter (mean ± S.E. (*error bars*)). No statistically significant difference was observed among the groups of mice with regard to the pixel number of sprouting or regenerating axons at any level along the rostrocaudal axis (using two-way repeated-measures ANOVA).

ter (Fig. 5, *A*, *C*, *E*, *G*, and *J*). However, no labeled axons were detected in the dorsal CST or the dorsolateral CST caudal to the injury site (Fig. 5, *B*, *D*, *F*, and *H*); this finding revealed that the lesion completely transected the axons in the descending CST. Moreover, for all groups, transverse sections of the gray or white matter below the injury site contained few or no BDA-labeled axons (Fig. 5, *B*, *D*, *F*, and *H*). Overall, the pattern of traced CST axons both above and below the injury site seemed comparable in all the groups. On the basis of quantitative analysis of the reconstructed spinal cord, we concluded that the areas caudal or rostral to the injury site did not significantly differ among the groups (Fig. 5, *I* and *J*). Thus, we obtained no evidence to show that the CST was regenerated after SCI in the PIR-B$^{-/-}$ or the NEP1–40-treated mice.

DISCUSSION

NgR and PIR-B have been identified as candidate receptors for three myelin-associated proteins (MAG, Nogo, and OMgp). Since then, these receptors have been considered potential therapeutic targets for promoting regeneration *in vivo*. In a previous study on NgR-null cerebellar neurons, antibody-mediated functional inhibition of PIR-B completely suppressed the inhibitory effects of MAG, Nogo, and OMgp on

neurite growth (5). Contrary to these results, we found that axonal regeneration in the CST was not enhanced in the PIR-B$^{-/-}$ mice after dorsal hemisection of the spinal cord. In addition, we found that treatment with NEP1–40, a Nogo-66 receptor antagonist, did not induce axonal regeneration in the CST, a finding that is consistent with one previous report (11) but conflicting with another (9). Further, neither the PIR-B$^{-/-}$ mice nor the NEP1–40-treated mice in our study exhibited enhanced recovery of locomotor activity after SCI. Our results challenge the view that the three myelin-associated proteins MAG, Nogo, and OMgp play a central role in transducing the inhibitory signals produced by myelin, as discussed recently (14). Moreover, these findings suggest that some other signals inhibiting axonal regeneration should be blocked and/or growth-stimulating signals should be provided to promote axonal regeneration in the CNS. For example, MAG and an N-terminal region of NogoA can act through an integrin-related mechanism (15), and MAG also signals via NgR2 and gangliosides (16). In addition, a number of other inhibitory molecules that could be playing a role exist in the CNS, *e.g.* repulsive guidance molecules, semaphorins, chondroitin sulfate proteoglycans, Wnts (1).

Although our findings are disappointing, the fact that axonal regeneration was not enhanced in the PIR-B$^{-/-}$ mice does not directly imply that PIR-B completely lacks a role in transducing the inhibitory signals for axonal regeneration *in vivo*. PIR-B is known to modulate immune responses by inhibiting the intracellular signaling in B cells and myeloid cells, and PIR-B$^{-/-}$ mice exhibit impaired maturation of dendritic cells and hyperactivated B cells and myeloid cells. Further, immunization of these mice with T-dependent antigens augments the humoral responses mediated by T helper type 2 cells (8). This role of PIR-B in the immune system, which is presumably implicated in the pathophysiology of neuronal injuries, suggests the functional significance of PIR-B in SCI.

PIR-B$^{-/-}$ mice exhibit an extended duration of experience-dependent ocular dominance plasticity during development (7); this indicates that PIR-B inhibits plasticity. A previous study revealed that the immunostaining of PIR-B is often adjacent to but rarely overlapping with that of the presynaptic proteins synaptophysin or synapsin (7), suggesting that PIR-B is localized at or beyond neural synapses. Further, in sections of the cerebral cortex, the PIR-B-alkaline phosphatase fusion protein is detected in association with the cell bodies and dendrites of cortical pyramidal neurons. We also reported that corticospinal neurons expressed PIR-B (13). In addition, we found that interneurons associated with the BDA-labeled CST in the spinal cord were immunoreactive for PIR-B. Therefore, plastic changes in the interneurons, as well as the axons of corticospinal neurons, may be enhanced in PIR-B$^{-/-}$ mice, although the quantitative measurement of those changes is technically challenging. However, because the recovery of locomotor activity after SCI was not significantly promoted in the PIR-B$^{-/-}$ mice in this study, we hypothesize that plasticity changes in the interneurons may have at best played only a minor role in rewiring the injured neural network in our model. It should also be noted that the behavioral tests we performed are not specific for the function of the CST. Therefore, our data suggest that the tracts for the motor function did not regenerate functionally in the absence of PIR-B.

The signal transduction mechanism by which PIR-B inhibits axonal growth remains to be elucidated, although the signals downstream of NgR have been well characterized (1). The cytoplasmic domain of PIR-B contains three immunoreceptor tyrosine-based inhibitory motifs and one immunoreceptor tyrosine-based inhibitory motif-like sequence. When these sites are phosphorylated, Shp-1 and Shp-2 phosphatases are recruited to PIR-B, which in turn modulates signal transduction pathways in the immune system (6). This indicates that Shp-1 and Shp-2 may play a role in the inhibition of axonal growth. Thus, tyrosine kinases like those of the Trk family, which promote the survival, differentiation, and axonal growth of neurons, are possible targets of Shp-1 and Shp-2. Future studies should aim to elucidate the molecular mechanisms underlying the functions of PIR-B in neurons. In summary, our findings indicate that PIR-B deletion does not enhance either CST regeneration beyond the lesion site or the recovery of locomotor activity after dorsal hemisection of the spinal cord.

Acknowledgment—We thank Dr. Shusaku Omoto for technical assistance and advice.

REFERENCES

1. Yiu, G., and He, Z. (2006) *Nat. Rev. Neurosci.* **7,** 617–627
2. Madura, T., Yamashita, T., Kubo, T., Fujitani, M., Hosokawa, K., and Tohyama, M. (2004) *EMBO Rep.* **5,** 412–417
3. Kim, J. E., Liu, B. P., Park, J. H., and Strittmatter, S. M. (2004) *Neuron* **44,** 439–451
4. Zheng, B., Atwal, J., Ho, C., Case, L., He, X. L., Garcia, K. C., Steward, O., and Tessier-Lavigne, M. (2005) *Proc. Natl. Acad. Sci. U.S.A.* **102,** 1205–1210
5. Atwal, J. K., Pinkston-Gosse, J., Syken, J., Stawicki, S., Wu, Y., Shatz, C., and Tessier-Lavigne, M. (2008) *Science* **322,** 967–970
6. Takai, T. (2005) *Immunology* **115,** 433–440
7. Syken, J., Grandpre, T., Kanold, P. O., and Shatz, C. J. (2006) *Science* **313,** 1795–1800
8. Ujike, A., Takeda, K., Nakamura, A., Ebihara, S., Akiyama, K., and Takai, T. (2002) *Nat. Immunol.* **3,** 542–548
9. Li, S., and Strittmatter, S. M. (2003) *J. Neurosci.* **23,** 4219–4227
10. GrandPré, T., Li, S., and Strittmatter, S. M. (2002) *Nature* **417,** 547–551
11. Steward, O., Sharp, K., Yee, K. M., and Hofstadter, M. (2008) *Exp. Neurol.* **209,** 446–468
12. Steward, O., Zheng, B., Tessier-Lavigne, M., Hofstadter, M., Sharp, K., and Yee, K. M. (2008) *J. Neurosci.* **28,** 6836–6847
13. Omoto, S., Ueno, M., Mochio, S., Takai, T., and Yamashita, T. (2010) *J. Neurosci.* **30,** 13045–13052
14. Silver, J. (2010) *Neuron* **66,** 619–621
15. Hu, F., and Strittmatter, S. M. (2008) *J. Neurosci.* **28,** 1262–1269
16. Schnaar, R. L., and Lopez, P. H. (2009) *J. Neurosci. Res.* **87,** 3267–3276